

A Conflicts-free, Speed-lossless KAN-based Reinforcement Learning Decision System for Interactive Driving in Roundabouts

Zhihao Lin^{1†}, Zhen Tian^{1†}, Qi Zhang², Ziyang Ye³, Hanyang Zhuang⁴, *Member, IEEE*, and Jianglin Lan^{1§*}

Abstract—Safety and efficiency are crucial for autonomous driving in roundabouts, especially in the context of mixed traffic where autonomous vehicles (AVs) and human-driven vehicles coexist. This paper introduces a learning-based algorithm tailored to foster safe and efficient driving behaviors across varying levels of traffic flows in roundabouts. The proposed algorithm employs a deep Q-learning network to effectively learn safe and efficient driving strategies in complex multi-vehicle roundabouts. Additionally, a KAN (Kolmogorov-Arnold network) enhances the AVs’ ability to learn their surroundings robustly and precisely. An action inspector is integrated to replace dangerous actions to avoid collisions when the AV interacts with the environment, and a route planner is proposed to enhance the driving efficiency and safety of the AVs. Moreover, a model predictive control is adopted to ensure stability and precision of the driving actions. The results show that our proposed system consistently achieves safe and efficient driving whilst maintaining a stable training process, as evidenced by the smooth convergence of the reward function and the low variance in the training curves across various traffic flows. Compared to state-of-the-art benchmarks, the proposed algorithm achieves a lower number of collisions and reduced travel time to destination.

Index Terms—Roundabout, interactive driving, reinforcement learning, autonomous vehicle, Kolmogorov-Arnold Network.

I. INTRODUCTION

AS urban roadways evolve, roundabouts have significantly increased the vehicle distribution and road capacity [1]. Compared to other crucial traffic scenarios, roundabouts have been verified to offer fewer conflicts [2]. However, the safety issue becomes more pronounced in high-traffic roundabouts, which has a higher potential for crashes [3]. The design of roundabouts varies for cities of different scales [4]. Typically, a roundabout is a type of circular intersection created to enable a smooth flow of traffic, characterized by a central island that is not meant for vehicular access [5]. In standard

roundabouts, the direction of travel is set—either clockwise or counterclockwise—simplifying the interaction complexities. The essential driving maneuvers in a roundabout include entering, lane selection, circulating, lane-changing, and exiting. Both merging into and exiting from the roundabout require interaction between the host vehicles and surrounding human-driven vehicles (HDVs), with host vehicles making self-optimized decisions by interpreting the intentions of other drivers. Choosing the correct lane allows host vehicles to maneuver with greater flexibility and efficiency. The lane-changing process obliges host vehicles to carefully monitor the state of surrounding HDVs to avoid possible collisions. Precise control is essential to adhere to the generated trajectories throughout the driving process. Thus, during navigation in roundabouts, host vehicles must have the ability to select the appropriate lane, monitor nearby entities and the environment, avoid collisions, and precisely control their movement.

Autonomous vehicles (AVs) can significantly reduce safety incidents that stem from human errors such as fatigue, distraction, and delayed reactions [6]. AVs are also capable of computing optimal decision-making solutions more swiftly than human drivers, thereby enhancing traffic efficiency [7]. Notably, AVs can enhance the capacity of roundabouts [8]. With the advent of AVs, whose amount is expected to exceed 50 million by 2024 [9], modern roundabout designs are increasingly accommodating AVs to address the challenges of safe control and interaction with HDVs [10]. Therefore, it is essential to ensure the safe operation of AVs in high-traffic roundabouts, particularly when they interact with HDVs [11]. Control strategies for connected autonomous vehicles (CAVs) are meticulously crafted to prioritize safety and efficiency in interactive driving situations [12]. Contemporary roundabout designs increasingly accommodate the operational needs of AVs, optimizing traffic flow and improving safety [13].

Existing studies on the interaction between AVs, CAVs, and HDVs in roundabouts can be broadly categorized into model-based and learning-based approaches. Model-based methods, such as game theory, have been widely used to model the decision-making process in interactive driving scenarios. Different driving behaviors in game processes can be modeled by adjusting the ratios of safety, efficiency, and driving comfort [14]. However, works using game process often rely on simplified environment and may not be able to handle the complex and dynamic nature of real-world roundabout scenarios [15], [16]. Other model-based frameworks face limitations due to the simplistic design of roundabouts, the low number

*This work was supported in part by the China Scholarship Council Ph.D. Scholarship for 2023-2027 (No.202206170011), in part by the Leverhulme Trust Early Career Fellowship (ECF-2021-517), and in part by the UK Royal Society International Exchanges Cost Share Programme (IEC\NSFC\223228).

¹Zhihao Lin, Zhen Tian and Jianglin Lan are with James Watt School of Engineering, University of Glasgow, Glasgow G12 8QQ, United Kingdom

²Qi Zhang is with Faculty of Science, University of Amsterdam, Science Park 904, 1098 XH Amsterdam, Netherlands

³Ziyang Ye is with School of Computer and Mathematical Sciences, The University of Adelaide, South Australia 5005, Australia

⁴Hanyang Zhuang is with University of Michigan-Shanghai Jiao Tong University Joint Institute, Shanghai Jiao Tong University, Shanghai, 200240, China

[§]Corresponding author. Jianglin Lan (e-mail: jianglin.lan@glasgow.ac.uk)

[†] Equal contribution

of vehicles involved, and the limited generalization as only an abnormal roundabout is focused [17], [18].

Learning-based approaches, such as machine learning and deep reinforcement learning (DRL), have shown great potential in complex interactive driving in roundabouts. Machine learning techniques have been used to explore safe and efficient interaction between AVs and HDVs [19]. However, these machine learning-based methods often require a large amount of labeled data and struggle to generalize to unseen scenarios. DRL, on the other hand, allows for extensive exploration of strategies in complex interactive environments. Therefore, DRL is well-suited for the interactive driving in roundabouts. By learning from experience, DRL-based controllers can balance safety and efficiency in dense traffic scenarios.

Several DRL algorithms have been applied to autonomous driving, including Deep Deterministic Policy Gradient (DDPG) [20], Proximal Policy Optimization (PPO) [21], and deep Q-learning network (DQN) [22]. DDPG is well-suited for continuous action spaces, but its advantages may not be fully exploited in complex tasks with discrete decisions, such as driving in the roundabout [23]. PPO has been used to develop intelligent driving strategies that balance safety and efficiency in dense highway traffic [24]. However, PPO's on-policy learning mode may be inefficient in utilizing historical data, which is crucial for approximating strategies in complex environments like roundabouts.

DQN has been effectively applied in various traffic simulations and is adept at tasks similar to roundabout navigation, such as intersection management [25]. DQN's discrete action framework directly applies to tasks like proper lane selection in roundabouts without the need for action discretization. Additionally, DQN applies experience replay to relearn from past experiences, achieving more efficient use of historical data. Furthermore, DQN tends to be less computationally demanding [26]. The recently proposed Kolmogorov-Arnold Network (KAN) has improved performance compared to traditional multi-layer perceptrons [27]. KAN uses the B-spline function to replace the linear layer in the multi-layer perceptron, which can adaptively adjust the feature extraction method of each neuron. It can flexibly change the shape of the kernel function to learn key feature patterns related to the task, which improves the adaptability and generalization performance in different environments.

To solve the complex driving in roundabouts, this paper proposes to integrate KAN with DQN (K-DQN) to enhance the decision-making and learning capabilities of AVs in complex roundabout scenarios. The K-DQN leverages the advantages of both DQN and KAN, enabling AVs to learn robust and efficient driving strategies through interaction with the environment. For conflict-free driving, we introduce an action inspector applied to time to collision (TTC) [28] to assess the relative collision risks between the AV and other HDVs. By replacing dangerous actions that may cause collisions with safe actions, our proposed method can decrease the ego vehicle collision rates with neighboring vehicles (NVs) during training. For proper lane selection, we introduce a route planner that considers the number of HDVs and the available free-driving space in each lane. For precise control of planned trajectories, we

implement model predictive control (MPC) to allow the AV to navigate with precision and robustness.

The main contributions of this paper are summarized as follows:

- We introduce a novel KAN-based DQN (K-DQN) to improve AVs' decision-making in complex roundabouts. By integrating KAN with spline-based activation functions, the K-DQN boosts observation and decision-making capabilities, leading to enhanced training convergence, reduced collisions, and increased average speeds.
- We propose an action inspector and a route planner to reduce collisions and enhance driving efficiency. The action inspector mitigates collision risks with HDVs, and the route planner optimizes lane selection for safety and space, significantly reducing collisions across various traffic flows compared to benchmarks.
- We integrate model predictive control (MPC) with K-DQN to convert planned actions into safe, smooth control commands, thereby enhancing journey safety and robustness. Our integrated solution adeptly manages diverse roundabout traffic flows, showing improved speed stability and efficiency over current benchmarks.
- We present mathematical analysis and experimental demonstrations to substantiate the superior performance of our K-DQN over traditional DQN methods. Extensive simulations confirm robustness and efficiency of our approach and its advantages over benchmarks.

The rest of this paper is organized as follows: Section II presents the problem statement and system structure; Section III describes the enhanced KAN-based DQN; Section IV introduces the action inspector and route planner; Section V presents the MPC design; Section VI provides the simulation results with analysis; Section VII draws the conclusion.

II. PROBLEM STATEMENT AND SYSTEM STRUCTURE

A. Problem Statement

The previous section underscored the significant attention given to studies on the interactive driving of AVs with HDVs in roundabouts. However, it is challenging in the integrated process of decision-making, path planning, and control for AVs to navigate roundabouts amid the varied complexity presented by HDVs. Interactions with HDVs, which can be randomly and densely distributed along both the inner and outer boundaries of roundabouts, frequently result in unexpected outcomes, such as conflicts and inefficient driving. Unlike straight or other curvy roads, roundabouts present unique challenges in making safe and efficient decisions due to their complex network of entrances and outlets. As illustrated in Fig. 1, there are four ports, each divided by a center white line into two half-ports—an entrance and an outlet. In this study, the right half-port of each is considered an entrance, while the left half-port serves as an outlet. The unpredictability of HDVs' intended outlets and their various maneuvers exacerbates the challenges for AVs in ensuring safe passage. Moreover, satisfactory driving considerations encompass not only safety but also efficiency, which involves minimizing the total driving time of an AV to a designated

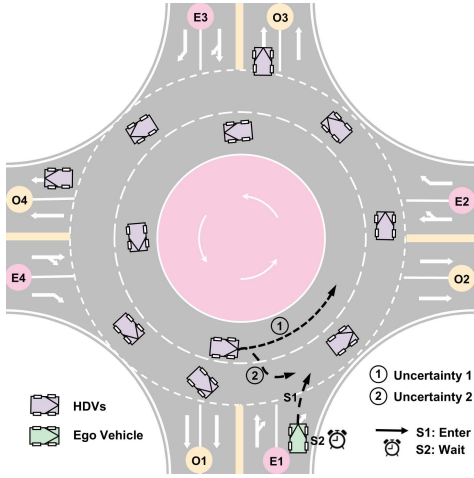


Fig. 1: The four-entrance, four outlet, and two-lane roundabout and an example of the first collision scenario with uncertainties of a autonomous vehicle.

outlet. The diverse and unpredictable actions of HDVs within the roundabout complicate the ability of AVs to achieve these goals simultaneously. This paper considers a double-lane roundabout without signal lights, featuring both HDVs and AVs as participants. In the modeled roundabout, HDVs are categorized into two types: those initially present within the roundabout and those merging into it. Three potential collision situations have been identified in Fig. 1, Fig. 2(a), and Fig. 2(b), respectively.

In Fig. 1, the first potential collision scenario is illustrated, where an AV is positioned at an entrance, while an HDV in the outer lane approaches the same entrance. This scenario leaves the AV with a decision influenced by the uncertain speed of the HDV. The AV has two options: to wait for the HDV to pass, thereby increasing its travel time, or to merge immediately, risking a collision, particularly if the relative velocity is low and the distance between the AV and HDV is minimal.

Figure 2 demonstrates the second potential collision scenario, in which the AV is navigating toward the same entrance from which an HDV is attempting to merge into the roundabout. This situation sets the stage for a possible collision if both vehicles attempt to occupy the entrance simultaneously.

Figure 2(b) illustrates the third potential collision scenario, which occurs when the AV wishes to exit from the inner lane but encounters an HDV in the adjacent outer lane. The AV has three options: overtaking the HDV with potential collision risks, following the HDV to reduce these risks, or staying in the current lane to wait for another opportunity to change lanes. These scenarios illustrate the high complexity and uncertainty that AVs face when engaging in interactive driving with surrounding HDVs in roundabouts.

B. System Structure

This paper primarily addresses the safety and efficiency of AVs from their entry to exit in roundabouts, taking into account the variable distribution and number of HDVs present. We consider varying traffic flows in the roundabout, from

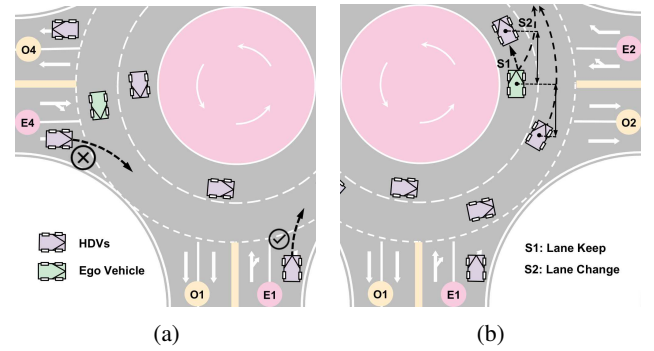


Fig. 2: Several challenging scenarios in the roundabout: (a) The second potential collision scenario; (b) The third potential collision scenario.

low to high density, and evaluate the system's adaptability to these changes. To adapt to varying traffic flows, the proposed system requires a combination of techniques. First, the agent is required to adapt to various driving scenarios with different traffic densities. Second, the real-time changes in the environment is required to make safe and efficient decisions even in highly dynamic scenarios. Finally, the smooth and safe navigation is needed through the driving in roundabout.

To solve the above problems, the proposed KAN-based, conflict-avoidance, and proper-lane-detection DRL system is designed, as depicted in Fig. 3. This system comprises four key components: the environment, decision network, safety and efficiency mechanism, and robust control. The environment module updates the state of AVs based on the generated control commands and also generates a reward at each step to assess the value of the selected action. The decision network makes safe and efficient decisions for each step. The safety and efficiency mechanism comprises two components: the route planner and the action inspector. The former is activated during the initial merge into the roundabout, guiding AVs to select a lane that ensures sufficient driving space and safety. The latter assesses and mitigates collision risks with HDVs. For robust control, MPC is implemented to translate planned actions into safe and smooth control commands, thus enhancing safety and robustness throughout the journey.

Besides the normal driving, the system uses action inspector to detect their presence and take related response to emergency situations. The AV will choose actions that allow the emergency vehicle to pass safely and quickly, such as moving to the outer lane or slowing down. The route planner module will also adjust its path to minimize interference with the emergency vehicle's trajectory.

III. KAN-ENHANCED DQN METHOD

The K-DQN network includes a replay memory, a KAN-Q-network, and a target Q-network. The KAN-Q-network, featuring a robust and precise learning process and a Q-network, processes data from the environment to generate gradient-based updates. This network is tasked with observing the surrounding HDVs and calculating the Q-value for making safe and efficient decisions. The target Q-network has the

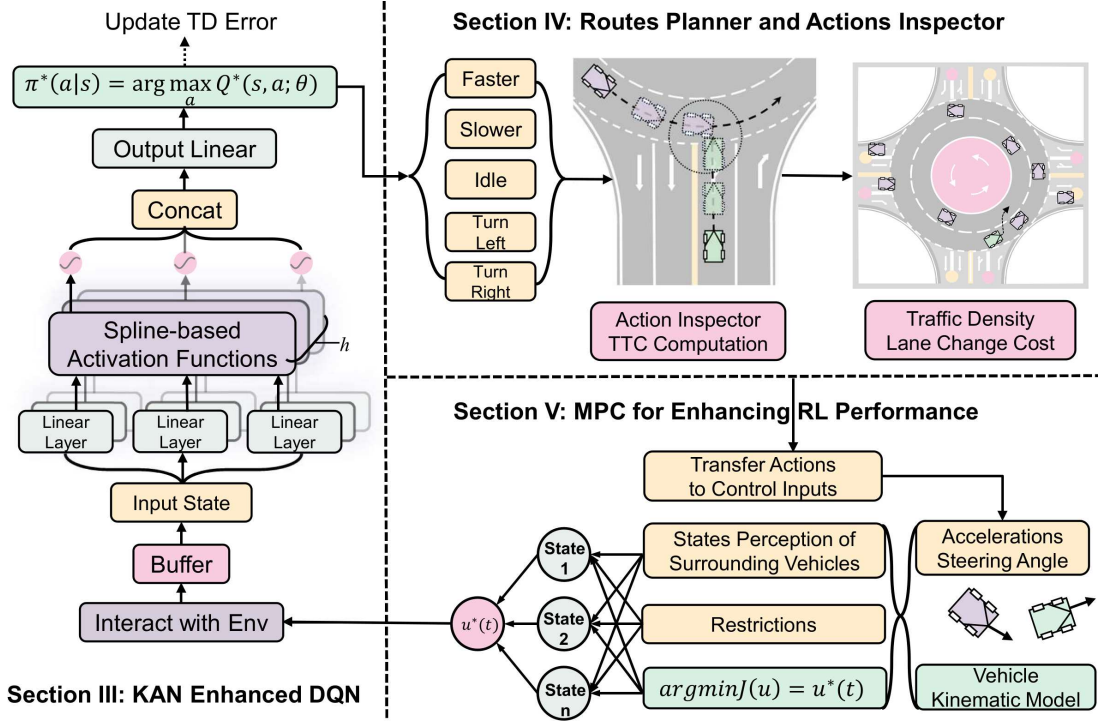


Fig. 3: The KAN-based, conflict-avoidance, and proper-lane-detection DRL system.

same structure as the KAN-Q-network, but its parameters are updated less frequently. The target Q-network helps to mitigate the issue of oscillations or divergence in the learning process. The parameters of the target Q-network are periodically synchronized with those of the KAN-Q-network to ensure that the target values remain consistent with the learned Q-values. To provide a clear understanding of the variables used in the mathematical derivations of K-DQN, we summarize their descriptions in Table I. This table includes the variables related to the KAN-Q-network and the approximation theory used.

A. Basic DQN

DQN combines deep learning with Q-learning, a reinforcement learning algorithm to address problems with high-dimensional state spaces. The core idea behind DQN is using a deep neural network to approximate the optimal action-value function $Q^*(s, a)$, which represents the maximum expected return for taking action a in state s .

The two key components of DQN are experience replay and target networks. Experience replay stores the agent's past experiences (s_t, a_t, r_t, s_{t+1}) in a replay buffer, allowing the agent to learn from past experiences multiple times, which stabilizes the learning process. The target network is a separate neural network used to compute the target Q-values during training. The parameters of the target network are periodically synchronized with the main Q-network. This helps to stabilize the learning process by reducing the correlation between the target Q-values and the current Q-values.

In Q-learning, the Q-value update rule is given by

$$Q(s_t, a_t) \leftarrow Q(s_t, a_t) + \alpha (r_t + \gamma \max_a Q(s_{t+1}, a) - Q(s_t, a_t)) \quad (1)$$

TABLE I
VARIABLES USED IN THE MATHEMATICAL DERIVATIONS

| Variable | Description |
|-------------------------------|--|
| s_t | State at time step t |
| a_t | Action at time step t |
| r_t | Reward at time step t |
| $Q(s, a; \theta)$ | Approximate action-value function with parameters θ |
| $Q^*(s, a)$ | Optimal action-value function |
| θ | Parameters of the current Q-network |
| θ' | Parameters of the target Q-network |
| α_i, β_i | Learnable coefficients in the KAN activation function |
| λ_1, λ_2 | Regularization coefficients in the KAN architecture |
| $\mathcal{L}(\theta)$ | Loss function for training the Q-network |
| γ | Discount factor |
| \mathbb{E} | Expectation operator |
| $f(x)$ | Output from the KAN layer |
| W | Weights of the output layer |
| b | Bias of the output layer |
| j | Index of the output layer neuron |
| n | Total number of output layer neurons |
| $\Phi_{L,i,j}$ | Spline functions in the approximation theory |
| $\Phi_{L,i,j}^G$ | k -th order B-spline functions in the approximation theory |
| C | Constant in the approximation theory |
| G | Grid size in the approximation theory |
| L_b | Lipschitz constants for activation function |
| L_{spline} | Lipschitz constants for spline functions |
| L_{Q^*} | Lipschitz constant for the optimal action-value function |
| ε | Approximation error |
| $\alpha_{\max}, \beta_{\max}$ | Maximum values of α_i and β_i |

where $Q(s_t, a_t)$ is the Q-value of executing action a_t in state s_t at time step t , α is the learning rate, r_t is the immediate reward obtained after executing a_t at time step t , γ is the discount factor to balance the importance of immediate and future rewards, and $\max_a Q(s_{t+1}, a)$ is the maximum Q-value of all possible actions in the next state s_{t+1} at time step $t+1$.

During the training process, we define the target value y as

$$y = r_t + \gamma \max_{a'} Q(s_{t+1}, a'; \theta') \quad (2)$$

where y is the ideal (target) Q-value of the current action calculated from the Bellman equation at time step t , and $\max_{a'} Q(s_{t+1}, a'; \theta')$ is the maximum Q-value of all possible actions a' in the next state s_{t+1} at time step $t + 1$, estimated using parameters θ' . It is important to note that variables with subscript t represent values at time step t , while variables without subscript t represent values in a general sense.

We use the difference between the predicted Q-value $Q(s_t, a_t; \theta)$ at time step t and the target value y to design the loss function

$$\mathcal{L}(\theta) = \mathbb{E} [(y - Q(s_t, a_t; \theta))^2] \quad (3)$$

where θ is the parameters of the target network and \mathbb{E} denotes the average expectation over all possible state-action pairs (s_t, a_t) encountered during training.

In the DQN framework, the objective is to minimize the loss function $\mathcal{L}(\theta)$. Once the loss is calculated, the Q-network's weights are updated in the opposite direction of the gradient to minimize the loss. The gradient $\frac{\partial \mathcal{L}}{\partial \theta}$ for updating the parameters in the DQN is derived as

$$\frac{\partial \mathcal{L}}{\partial \theta} = \mathbb{E} \left[2(Q(s_t, a_t; \theta) - y) \frac{\partial Q}{\partial \theta} \right] \quad (4)$$

with y given in (2).

The gradients play a crucial role in updating the parameters of the DQN. They represent the rate of change of the loss function with respect to the Q-network's parameters, indicating the direction in the parameter space that would lead to the steepest decrease in the loss function. By computing these gradients, we can determine how to adjust the parameters to minimize the loss function most effectively. Specifically, we update the parameters θ using the gradient descent algorithm, moving in the negative gradient direction:

$$\theta \leftarrow \theta - \alpha \frac{\partial \mathcal{L}}{\partial \theta} \quad (5)$$

where α is the learning rate that controls the step size of each update. This update process is iterated until the loss function converges to a sufficiently low value, at which point the Q-network's predictions will be close to the target values.

B. Structure of KAN

The core of the KAN architecture consists in using spline-based activation functions of the form:

$$f(x_i; \theta_i, \beta_i, \alpha_i) = \alpha_i \cdot \text{spline}(x_i; \theta_i) + \beta_i \cdot b(x_i) \quad (6)$$

where x_i is the input to the i -th neuron, $\text{spline}(x_i; \theta_i)$ represents the spline function parameterized by coefficients θ_i , $b(x_i) = \text{SiLU}(x_i) = x_i / (1 + e^{-x_i})$ is an activation function, and α_i and β_i are learnable coefficients. Spline functions are piecewise polynomial functions with high expressiveness and can approximate any continuous function. By adjusting the parameters and coefficients of the spline function, KAN can approximate various complex nonlinear functions.

The coefficients of the spline, θ_i , are updated through gradient descent methods using the loss function $\mathcal{L}(\theta)$ in (3). The update law is

$$\theta_i^{(t+1)} = \theta_i^{(t)} - \eta \frac{\partial \mathcal{L}}{\partial \theta_i} \quad (7)$$

where η is the learning rate. KAN also employs regularization strategies to mitigate the risk of overfitting:

$$\mathcal{R}(\theta) = \lambda_1 \sum_i |\theta_i| + \lambda_2 \sum_i \sum_{j \neq i} |\theta_i - \theta_j| \quad (8)$$

where $\mathcal{R}(\theta)$ is the regularization term added to $\mathcal{L}(\theta)$, which can control the complexity of the model whilst fitting the data and improve the generalization ability of the model. λ_1 and λ_2 are regularization coefficients. The L_1 regularization term, $\lambda_1 \sum_i |\theta_i|$, promotes sparsity in the parameter matrix. Another L_1 regularization term, $\lambda_2 \sum_i \sum_{j \neq i} |\theta_i - \theta_j|$, ensures smoothness in the parameter values across different neurons, facilitating model stability and preventing drastic changes in the output for minor fluctuations in the input data.

KAN also adopts parameter sharing among neurons defined as follows:

$$\theta_{\text{shared}} = \frac{1}{N_{\text{group}}} \sum_{i \in \text{group}} \theta_i \quad (9)$$

where group includes indices of neurons sharing parameters, and N_{group} is the number of neurons in this group. The shared parameters, θ_{shared} , reduce the overall model complexity by averaging the parameters of neurons within the same group, enhancing computational efficiency and potentially improving the model's generalization capabilities over similar features.

These elements of the KAN architecture collectively enhance the flexibility and efficiency of the learning process, whilst ensuring robustness against overfitting and maintaining high performance across reinforcement learning tasks.

C. KAN Enhanced DQN

The integration of KAN within DQN, termed K-DQN, enables the network to better approximate the Q-function, especially in scenarios with complex action dynamics and reward functions. This capability translates into more robust learning and improved policy development in DRL tasks. To demonstrate why using the KAN network combined with DQN is superior to combining it with other reinforcement learning frameworks, it is essential to analyze the core differences in how these algorithms handle environments and tasks, as well as the characteristics of KAN activation functions.

To formulate the roundabout driving problem as a Markov Decision Process, we define the following key components:

State Space: The state space \mathcal{S} consists of the ego vehicle's position, velocity, and heading, as well as the relative positions, velocities, and headings of the surrounding vehicles within a certain range. The state at time t is represented as

$$s_t = [p_{\text{EV}}(t), v_{\text{EV}}(t), h_{\text{EV}}(t), p_{\text{NV}}^i(t), v_{\text{NV}}^i(t), h_{\text{NV}}^i(t)]^\top \quad (10)$$

where $p_{\text{EV}}(t)$, $v_{\text{EV}}(t)$, and $h_{\text{EV}}(t)$ denote the position, velocity, and heading of the ego vehicle at time t , and $p_{\text{NV}}^i(t)$, $v_{\text{NV}}^i(t)$,

and $h_{\text{NV}}^i(t)$ represent the position, velocity, and heading of the i -th neighboring vehicle at time t .

Action Space: The action space \mathcal{A} is discrete and consists of five high-level actions: faster, slower, idle, turn right, and turn left.

Reward Function: The reward function $r : \mathcal{S} \times \mathcal{A} \rightarrow \mathbb{R}$ is designed to encourage the ego vehicle to drive safely and efficiently through the roundabout. The reward function is defined as a weighted sum of several components:

$$r(s_t, a_t) = w_1 r_c + w_2 r_s + w_3 r_{\text{lc}} + w_4 r_h + w_5 r_a \quad (11)$$

where r_c penalizes collisions, r_s rewards driving at high speeds, r_{lc} penalizes excessive lane changes, r_h encourages maintaining a safe distance from surrounding vehicles, and r_a rewards reaching the target exit. The weights w_1, \dots, w_5 balance the importance of each component.

By using (6), the goal is to directly approximate the optimal action-value function

$$\begin{aligned} Q(s, a; \theta) &= \sum_j W_j^T f(x) + b \\ &= \sum_{j \in [1-n]} \sum_{i=1}^m (\alpha_i \cdot \text{spline}(x_i; \theta_i) + \beta_i \cdot b(x_i)) + b \\ &= \sum_{j \in [1-n]} \sum_{i=1}^m (\alpha_i \cdot \text{spline}((s, a)_i; \theta_i) + \beta_i \cdot b((s, a)_i)) + b \end{aligned} \quad (12)$$

where W and b are the weights and bias of the network, $f(x)$ is the output from the KAN layer, j is the index of the output layer neuron, and n is the total number of output layer neurons.

Theorem 1: (Approximation theory [27]) Suppose that a function $f(x)$ admits a representation $f = (\Phi_{L-1} \circ \Phi_{L-2} \circ \dots \circ \Phi_1 \circ \Phi_0)x$, where each part Φ_l is $(k+1)$ -times continuously differentiable. Then there exist k -th order B-spline functions Φ_l^G such that for any $0 \leq m \leq k$,

$$\|f - (\Phi_{L-1}^G \circ \Phi_{L-2}^G \circ \dots \circ \Phi_1^G \circ \Phi_0^G)x\|_{C^m} \leq CG^{-k-1+m} \quad (13)$$

where C is a constant and G is the grid size. The magnitude of derivatives up to order m is measured by the C^m -norm as

$$\|g\|_{C^m} = \max_{|\beta| \leq m} \sup_{x \in [0,1]^n} |D^\beta g(x)|. \quad (14)$$

We aim to prove that under the conditions of Theorem 1, DQN with KAN as the backbone network can effectively approximate the optimal action-value function $Q^*(s, a)$. Assume the true action-value function for taking action a in state s is $Q^*(s, a)$. Our goal is to find an approximation function $Q(s, a; \theta)$ that is as close as possible to $Q^*(s, a)$.

Considering the mean squared error properties of DQN and y given in (2), we have

$$\mathbb{E}[(Q(s_t, a_t; \theta) - Q^*(s_t, a_t))^2] = \mathbb{E}[(Q(s_t, a_t; \theta) - y)^2] + C \quad (15)$$

where $C = \mathbb{E}[(r_t + \gamma \max_{a'} Q(s_{t+1}, a'; \theta') - Q^*(s_t, a_t))^2]$ is a constant independent of θ . Therefore, minimizing the loss function $\mathcal{L}(\theta)$ is equivalent to minimizing the mean squared error between the approximate value function $Q(s_t, a_t; \theta)$ and the target value $r_t + \gamma \max_{a'} Q(s_{t+1}, a'; \theta')$.

When we use KAN as the backbone network in DQN, the optimization objective can be rewritten as

$$\min_{\theta} \mathbb{E}[(Q(s_t, a_t; \theta) - (r_t + \gamma \max_{a'} Q(s_{t+1}, a'; \theta')))^2]. \quad (16)$$

By using (12), $Q(s_t, a_t; \theta)$ can be defined as:

$$\begin{aligned} Q(s_t, a_t; \theta) &= \sum_j \sum_{i=1}^m (\alpha_i \cdot \text{spline}((s_t, a_t)_i; \theta_i) \\ &\quad + \beta_i \cdot b((s_t, a_t)_i)) + b. \end{aligned} \quad (17)$$

Since the spline functions and $\text{SiLU}(x)$ in (6) used in KAN are continuously differentiable, the conditions of Theorem 1 are satisfied. By applying Theorem 1, we can conclude that for any state-action pair (s, a) , there exists an optimal set of parameters θ^* such that $Q(s, a; \theta^*)$ in (17) can arbitrarily approximate the optimal action-value function $Q^*(s, a)$.

Theorem 2: Let $Q(s, a; \theta)$ be the approximate action-value function defined by (12), where the spline functions $\text{spline}(x; \theta)$ and the activation function $b(x)$ are Lipschitz continuous with Lipschitz constants L_{spline} and L_b , respectively. Assume that the optimal action-value function $Q^*(s, a)$ is also Lipschitz continuous with Lipschitz constant L_{Q^*} . Then, for any $\varepsilon > 0$, there exists a set of parameters θ^* such that

$$\|Q(s, a; \theta^*) - Q^*(s, a)\|_{\infty} \leq \varepsilon, \quad (18)$$

and for any $\theta \in \Theta$,

$$\|Q(s, a; \theta) - Q^*(s, a)\|_{\infty} \leq \varepsilon + C \|\theta - \theta^*\|_2 \quad (19)$$

where $C = \sqrt{m}(\alpha_{\max} L_{\text{spline}} + \beta_{\max} L_b)$, m is the number of basis functions used in the spline approximation, $\alpha_{\max} = \max_i \alpha_i$, and $\beta_{\max} = \max_i \beta_i$.

Proof: By the universal approximation theorem for spline functions [29], $\forall \varepsilon > 0$, there is a θ^* such that

$$\|Q(s, a; \theta^*) - Q^*(s, a)\|_{\infty} \leq \varepsilon. \quad (20)$$

For any $\theta \in \Theta$, we have

$$\begin{aligned} \|Q(s, a; \theta) - Q^*(s, a)\|_{\infty} &\leq \|Q(s, a; \theta) - Q(s, a; \theta^*)\|_{\infty} + \|Q(s, a; \theta^*) - Q^*(s, a)\|_{\infty} \\ &\leq \|Q(s, a; \theta) - Q(s, a; \theta^*)\|_{\infty} + \varepsilon. \end{aligned} \quad (21)$$

By the Lipschitz continuity of $\text{spline}(x; \theta)$ and $b(x)$, we obtain

$$\begin{aligned} \|Q(s, a; \theta) - Q(s, a; \theta^*)\|_{\infty} &\leq \sum_{j \in [1-n]} \sum_{i=1}^m (\alpha_i L_{\text{spline}} \|\theta_i - \theta_i^*\|_2 + \beta_i L_b \|\theta_i - \theta_i^*\|_2) \\ &\leq \sqrt{m}(\alpha_{\max} L_{\text{spline}} + \beta_{\max} L_b) \|\theta - \theta^*\|_2. \end{aligned} \quad (22)$$

Combining (21) and (22) gives (19). \square

Theorem 2 provides a quantitative bound on the approximation error between the learned action-value function $Q(s, a; \theta)$ and the optimal one $Q^*(s, a)$. The bound consists of two terms: (i) The universal approximation error ε , which can be made arbitrarily small by choosing a suitable θ^* . (ii) The term $C \|\theta - \theta^*\|_2$, which depends on the distance between the learned parameters θ and the optimal parameters θ^* . The Lipschitz continuity of the spline functions and the activation

function, as well as the bound on the coefficients α_i and β_i , ensure the stability and generalization of the learned action-value function. As the training progresses and θ approaches θ^* , the approximation error decreases, indicating the convergence of the learned action-value function to the optimal one.

Under Theorem 2, by minimizing the loss function (3), DQN combined with KAN can effectively approximate the optimal action-value function $Q^*(s, a)$, as demonstrated by:

$$\lim_{\theta \rightarrow \theta^*} \mathcal{L}(\theta) \rightarrow 0 \implies \lim_{\theta \rightarrow \theta^*} Q(s, a; \theta) \rightarrow Q^*(s, a). \quad (23)$$

The optimal policy π^* is derived from the optimal action-value function Q^* by selecting the action that maximizes Q^* for each state:

$$\pi^*(a | s) = \arg \max_a Q^*(s, a). \quad (24)$$

Therefore, K-DQN can approximate the optimal action-value function $Q^*(s, a)$ by optimizing over the loss function (3), and thus learn the optimal policy π^* . This demonstrates the effectiveness and superiority of KAN in enhancing DQN. The direct optimization approach of K-DQN, supported by the approximation theory and the quantitative error bound, enables K-DQN to better learn and optimize policies.

IV. ROUTES PLANNER AND ACTIONS INSPECTOR

This section introduces the mechanisms to ensure the safety and efficiency during the interactive driving in the roundabout. Three subsections are included: the driving rules of HDVs, the action inspector, and the route planner.

A. Driving Rules of HDVs

This subsection outlines the priority rules for HDVs operating within roundabouts, designed to maintain traffic flow and enhance safety. The rules are formulated to address typical scenarios encountered in roundabouts.

1) *Entry Rule:* When an HDV approaches a roundabout entrance, it must yield to any vehicle already passing through the entrance it intends to use. This rule ensures that vehicles inside the roundabout maintain a smooth flow and reduces potential entry conflicts.

$$\text{HDV}_{\text{entering}} \not\leftarrow \text{if } \exists \text{HDV}_{\text{passing}} \quad (25)$$

Once inside the roundabout, ego HDVs (EHDV) are required to adjust their speeds according to the Intelligent Driver Model (IDM) to maintain a safe distance from their immediate front HDV (FHDV) until they reach their intended exit. This adjustment is crucial for preventing rear-end collisions and ensuring steady traffic flow within the roundabout. The IDM following rule is formulated as

$$a_{\text{IDM}} = a_{\text{max}} [1 - (v_{\text{FHDV}}/v_e)^4 - (h^*/h)^2] \quad (26)$$

where a_{max} is the maximum acceleration of EHDV, v_{FHDV} is the velocity of FHDV, v_e is the expected velocity of EHDV, and h is the real gap between EHDV and FHDV. h^* is the desired gap between EHDV and FHDV with the formula

$$h^* = h_e + v_{\text{AV}} T_e - \frac{v_{\text{AV}} \Delta v}{2\sqrt{a_{\text{max}} c}} \quad (27)$$

where h_e is the expected space with FHDV, v_{AV} is the speed of the AV, T_e is the expected time gap, Δv is the velocity difference between EHDV and FHDV, and c is the comfortable deceleration.

2) *Inner Lane Following Rule:* HDVs in the inner lane of the roundabout must align their speeds with the nearest vehicle ahead, even if that vehicle is in the outer lane. This rule is intended to synchronize speeds across lanes and enhance the cohesive flow of traffic, particularly in multi-lane roundabouts.

B. Route Planner

The integrated route planner for the EV comprises initial-lane selection decisions, a path-planning algorithm, and a lane-change selection mechanism. The initial-lane selection is guided by the TTC metric for each lane, ensuring safety and efficiency from the start. The path planning algorithm employs a node-based shortest path calculation to determine the most optimal route. The lane-change selection mechanism is driven by a proposed lane change cost formula, facilitating effective and strategic lane changes.

1) *Initial-Lane Selection:* By computing the TTC between the ego vehicle and surrounding vehicles, the safety levels can be ensured and unsafe actions can be avoided. In this scenario, the more potential space for driving and safety are the major considerations, thus we calculate the TTC for the inner and outer lanes as follows:

$$\begin{aligned} \text{TTC}_{\text{inner}} &= \frac{\text{Distance to HDV}_{\text{inner}}}{\text{Speed of EV} - \text{Speed of HDV}_{\text{inner}}}, \\ \text{TTC}_{\text{outer}} &= \frac{\text{Distance to HDV}_{\text{outer}}}{\text{Speed of EV} - \text{Speed of HDV}_{\text{outer}}}. \end{aligned} \quad (28)$$

The obtained TTC of both lanes can then be used to make the initial-lane selection rules. This paper considers several situations: No HDVs present, One HDV in outer lane, One HDV in both lanes, and Multiple HDVs in both lanes. These scenarios are described as follows:

- **No HDVs present:** The lane selection rule is

$$\text{Lane}_{\text{selected}} = \text{Inner lane} \quad \text{if HDVs} = 0. \quad (29)$$

When no HDVs are present in the roundabout, the AV will directly select the inner lane due to its shorter radius, which reduces the distance from the entrance to the outlet.

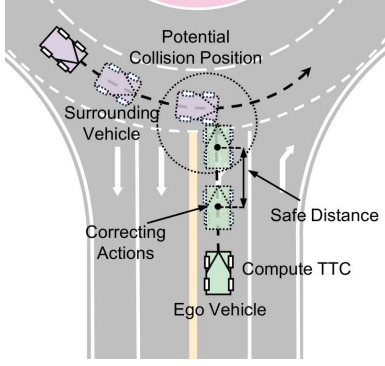
- **One HDV in outer lane:** Fig. 4(a) illustrates this scenario. In this scenario, the EV will compute the TTC to maintain a safe distance from surrounding vehicles and merge into the inner lane.

- **One HDV in both lanes:** As illustrated in Fig. 4(b), by evaluating the TTC of both lanes, the lane with the higher TTC is selected for safety and more driving space. If having equal TTC values, the inner lane is chosen to enhance efficiency. The rule is summarized as

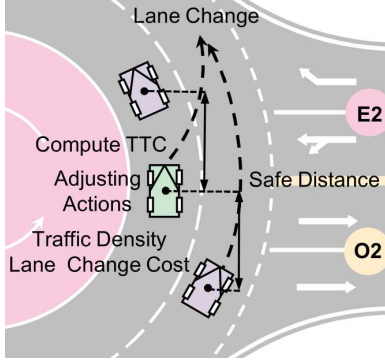
$$\text{Lane}_{\text{selected}} = \begin{cases} \text{Inner lane} & \text{if } \text{TTC}_{\text{inner}} \geq \text{TTC}_{\text{outer}} \\ \text{Outer lane} & \text{otherwise} \end{cases}. \quad (30)$$

If two HDVs have the same velocity but the inner-lane HDV is farther from the EV, the inner lane is selected.

- **Multiple HDVs in both lanes:** This scenario is most complex, as both inner-lane and outer-lane have two HDVs.



(a) Scenario with one HDV in the outer lane



(b) Scenario with one HDV in both lanes

Fig. 4: Lane selection cases. (a) shows the case with one HDV in the outer lane, requiring the EV to select the safest lane by the higher TTC; (b) shows the case with one HDV in both lanes, and the EV selects the lane by the higher TTC.

When multiple vehicles (in this paper more than 2 vehicles are defined as multiple case) are present in both lanes, a weighted decision based on TTC and Total Driving Time (TDT) to the outlet is used:

$$\begin{aligned} \text{TTC}_{\text{weighted}} &= w_1 \cdot \text{TTC}_{\text{nearest}} + w_2 \cdot \text{TDT}, \\ \text{TDT} &= \sum \text{Driving time of each HDV to EV's outlet.} \end{aligned} \quad (31)$$

The weights w_1 and w_2 are predetermined based on the traffic model preferences. The lane with the lower weighted score is selected to maximize safety and avoid the lane with longer total travel time of HDVs, which prevents the forward driving of AV. The entire initial-lane selection process is summarized in the Algorithm 1.

2) *In-Roundabout Lane Selection*: After entering the roundabout and selecting an initial lane, the next stage is path planning. We adopt a modified Breadth-First Search (BFS) [30] method that considers both distance and traffic conditions to compute the optimal path from a start point to a target within a graph structure, where nodes represent intersections in the road network, and edges represent drivable roads. The modified BFS algorithm uses a cost function that takes into account both the distance and traffic density:

$$C(e) = w_1 \cdot D(e) + w_2 \cdot \mathcal{D}(e) \quad (32)$$

Algorithm 1 Action Priority List for the EV

Input: L : The number index of lanes in the roundabout.

$\alpha_1, \alpha_2, \alpha_3, \alpha_4$: Coefficients for computing the priority scores based on the current situation. T_n : The number of prediction steps for trajectory planning. $A_{t,i}$: Set of feasible actions for vehicle i at time step t .

Output: P_t : Priority list of actions for the EV.

- 1: Determine the presence of HDVs in the roundabout.
 - 2: **if** no HDVs present **then**
 - 3: Select the inner lane.
 - 4: **else**
 - 5: Compute TTC for each HDV in both lanes.
 - 6: **if** one HDV in each lane **then**
 - 7: Choose lane having the highest TTC value,
 - 8: preferring inner lane if equal.
 - 9: **else if** multiple HDVs in both lanes **then**
 - 10: Use $\text{TTC}_{\text{weighted}}$ in (31) to select lane.
 - 11: **end if**
 - 12: **end if**
 - 13: Initialize action priority list P_t for the EV.
 - 14: **for** each feasible action a_{feasible} in $A_{t,i}$ **do**
 - 15: Compute the priority score of a_{feasible} .
 - 16: Add a_{feasible} to P_t according to its priority score.
 - 17: **end for**
-

where $C(e)$ is the cost of edge e , $D(e)$ is the distance of edge e , $\mathcal{D}(e)$ is the traffic density of edge e , and w_1 and w_2 are weight factors that determine the relative importance of distance and traffic density. $\mathcal{D}(e)$ is calculated by

$$\mathcal{D}(e) = N_e / L_e \quad (33)$$

where N_e is the number of vehicles on edge e , and L_e is the length of edge e . The modified BFS is formulated as

$$\text{BFS}(s, g) = \min\{p : s \rightarrow \dots \rightarrow g \mid p \in \text{Paths}(s, g)\} \quad (34)$$

where s is the start node, g is the goal node, and $\text{Paths}(s, g)$ is the set of all possible paths. The optimal path is given as

$$p^* = \arg \min_{p \in \text{Paths}(s, g)} \sum_{e \in p} C(e) \quad (35)$$

where p^* is the optimal path.

3) *Lane Selection Mechanism*: As the scenario illustrated in Fig. 4(b), traffic density (\mathcal{D}) and lane-change cost (\mathcal{C}), are computed. The computation of two parameters are as follows:

- **Traffic Density \mathcal{D}** is calculated by iterating over all vehicles to count the number on a specified node and lane, and adjusting the density value based on vehicles' relative positions, with closer vehicles having a higher weight. When the EV is at lane node n , the density is

$$\mathcal{D}(n, l) = \sum_{NV \in N_V} \mathbf{1}_{(NV.n=n \wedge NV.l=l)} - \mathbf{1}_{(NV.n=n \wedge NV.l \neq l)} \quad (36)$$

where n indicates the node, l indicates the lane, N_V is the set of neighbor vehicles, and $\mathbf{1}$ is the indicator function:

$$\mathbf{1}_{\text{condition}} = \begin{cases} 1 & \text{if the condition is true} \\ 0 & \text{otherwise} \end{cases}. \quad (37)$$

• **Lane Change Cost \mathcal{C}** is obtained by computing the distance between the controlled vehicle and other vehicles. The costs increase sharply if the distance is less than a threshold safety distance D_{safe} . The cost formula is

$$D(EV, NV) = \|p_{EV}(t) - p_{NV}(t)\|$$

$$\mathcal{C}(n, l) = \sum_{NV \in N_V} \frac{D_{safe}}{D(EV, NV)} \cdot \mathbf{1}_{(D(EV, NV) < D_{safe})} \quad (38)$$

where $D(EV, NV)$ is the distance between EV and NV, $p_{EV}(t)$ is EV's position at time step t , and $p_{NV}(t)$ is NV's position at time step t .

Based on the above parameters, the lane is selected using

$$\text{lane_choice} = \arg \min_{l \in \{0,1\}} (D(n, l) + \mathcal{C}(n, l)). \quad (39)$$

If the costs for both lanes are equal, the decision is further optimized based on the vehicle's current position. This approach enhances the efficiency and safety of vehicle control around a roundabout by integrating real-time traffic conditions with the potential risks of lane changes. By utilizing the modified BFS algorithm, the algorithm optimizes the selection of paths. Besides, the route planner employs an edge selection function, creating a comprehensive solution for autonomous vehicle navigation in roundabouts.

C. Action Inspector

Each ego vehicle (EV) plans its acceleration through the roundabout and it is encouraged to accelerate during driving. However, the collision risk should be measured. To this end, the EV would predict the trajectories of NVs when the distance between the EV and any NV is less than the (D_{safe}) for the EV to change lane safely as depicted in Fig. 4 (b).

If there are overlaps between EV's future trajectories and NVs' trajectories, the EV will use IDM (26) to follow the nearest preceding vehicles, and to synchronize with the overall traffic flow. The following mode would generate a penalty if the EV's velocity is below the expected velocity for more than three seconds. This mechanism enables the EV to avoid conflicts and understand the requirement to drive to the outlet as quickly as possible.

1) *Safety Margin Calculation*: This margin is used to guide decision-making when selecting driving actions. As vehicles maintain a wider angle relative to each other while in proximity, the likelihood of their paths intersecting decreases. Therefore, the safety margin for each vehicle's maneuver is defined as the minimum difference in relative angle, D_a , or the shortest time until a potential collision could occur.

$$\text{Safety Margin} = \min_{a \in A_{feasible}} D_{a,a,k} \quad (40)$$

where $A_{feasible}$ is the set of feasible actions and $D_{a,a,k}$ is the safety margin angle under action a at prediction time k .

2) *Decision-Making Criteria*: For each decision point, the AV will calculate safety margins for multiple options. If the safety margins are equivalent, the AV will prefer the lane that optimizes the route, typically the inner lane in roundabouts due to the shorter path length to the exit.

Algorithm 2 Action execution for EV in a Roundabout

Input: P_t : Priority list of actions for the EV, initialized and populated as per the previous algorithm.

Output: $a_{t,i}$: The optimal action for vehicle i at time step t , chosen and executed from the priority list.

```

1: while  $P_t$  is not empty do
2:    $a_t \leftarrow P_t[0]$ 
3:   for  $NV$  in  $N_V$  and  $D(EV, NV) \leq D_{safe}$  do
4:     if  $EV_{a_t}$  and  $NV$  trajectories overlap in  $T_n$  then
5:       if  $NV$  in same lane and in front then
6:         Use IDM (26) to follow FHDV; break
7:       else if  $NV$  in adjacent lane then
8:         Replace  $a_t$  with the next highest priority
           action in  $P_t$ .
9:       end if
10:    end if
11:  end for
12:  if no overlap then
13:    Execute  $a_t$ 
14:  end if
15:  Remove  $a_t$  from  $P_t$ 
16: end while

```

3) *Dangerous Action Replacement*: When the action inspector detects a dangerous action that may lead to a collision, it replaces the action with the next highest priority action from the list P_t . This process ensures that the EV always selects the safest possible action while still being efficient. If no safe action is found in P_t , the EV will use IDM to follow the nearest preceding vehicle until a safe action becomes available.

4) *Update Rule*: After each EV's action decision, the action with the next highest priority is selected. This process of actions inspector repeats until EV have safely navigated through the roundabout. The actions inspector helps the EV avoid conflicts by continuously replacing dangerous actions with safer alternatives, as summarized in the Algorithm 2.

In summary, the proposed route planner and action inspector provide a comprehensive solution for safe and efficient navigation of autonomous vehicles in complex roundabout scenarios. The route planner's initial lane selection based on TTC ensures a safe entry into the roundabout, while the modified BFS algorithm optimizes the path by considering both distance and traffic density. The lane selection mechanism, which incorporates traffic density and lane change costs, enables strategic and safe lane changes within the roundabout. The action inspector continuously monitors the safety of planned actions and replaces dangerous maneuvers with safer alternatives, minimizing the risk of collisions. By integrating global route planning with localized lane change decisions based on real-time traffic data, the proposed system demonstrates exceptional adaptability to varying traffic conditions.

V. MPC FOR ENHANCING DRL PERFORMANCE

This section introduces the robust control for AVs including the vehicle dynamic model and MPC. The MPC controller considers the vehicle dynamics, collision avoidance, and other

constraints in its optimization process. It predicts the future states of the EV and surrounding vehicles using the vehicle dynamic model and the actions of neighboring vehicles predicted by the DRL agent. The combination of DRL and MPC in the proposed framework brings several benefits: it allows the DRL agent to focus on high-level decisions while the MPC manages low-level controls; the MPC can correct any imperfections in the DRL agent's decisions to ensure safe and feasible actions; and MPC provides a reliable, interpretable control strategy based on clear vehicle dynamics and constraints.

The state of the EV at time step t is updated using

$$\begin{aligned} p_{EV}(t+1) &= p_{EV}(t) + v_{EV}(t) \cdot \cos(h_{EV}(t)) \cdot \Delta t \\ v_{EV}(t+1) &= v_{EV}(t) + u(t) \cdot \Delta t \\ h_{EV}(t+1) &= h_{EV}(t) + \frac{v_{EV}(t)}{L} \cdot \tan(\delta(t)) \cdot \Delta t \end{aligned} \quad (41)$$

where Δt is the sampling time, $v_{AV}(t)$ is the speed, $h_{AV}(t)$ is the heading angle, L is the wheelbase length, $u(t)$ is the acceleration, and $\delta(t)$ is the steering angle.

The following control input and collision avoidance constraints are applied to ensure safety and feasibility:

$$\begin{aligned} v_{\min} \leq v_{EV}(t) \leq v_{\max}, \quad a_{\min} \leq u(t) \leq a_{\max}, \\ \delta_{\min} \leq \delta(t) \leq \delta_{\max}, \quad \|p_{EV}(t) - p_{NV}(t)\| \geq D_{safe}. \end{aligned} \quad (42)$$

At time step t , the optimal solutions $u^*(t)$ and $\delta^*(t)$ are obtained by solving the optimization problem:

$$\begin{aligned} \min J_c \\ \text{s.t. (41), } 0 < v_{AV}(k) \leq v_{\max}, a_{\min} \leq u(k) \leq a_{\max}, \\ \delta_{\min} \leq \delta(k) \leq \delta_{\max}, NV \in N_V, k \in [0, N_p - 1] \end{aligned} \quad (43)$$

with the cost function $J_c = \sum_{k=0}^{N_p-1} (v_{AV}(k) - v_{AV}^*)^2 + \sum_{k=0}^{N_p-1} \sum_{i=1}^{N_v} (\|p_{SV}^i(k) - p_{AV}^i(k)\| - D_{safe})^2 + \lambda \sum_{k=0}^{N_c-1} u^2(k)$. N_p and N_c represent the prediction horizon and control horizon, respectively. N_p is the prediction horizon and N_c is the control horizon. $v_{AV}^*(k)$ is the target speed, N_v is the number of NVs, and λ is a weighting factor for the acceleration penalty. In our experiments, we set N_p as 10 and the N_c as 5. The entire control process is summarized in Algorithm 3.

VI. SIMULATION RESULTS

In this section, we assess the performance of the proposed K-DQN algorithm by evaluating its training efficiency and collision rate within the roundabout driving scenario, within the roundabout driving scenario depicted in Section II. The inner roundabout's road radius is 40 meters, and the outer roundabout's road radius is 48 meters, with both lanes having a width of 4 meters. Vehicles that exit the roundabout will be removed from the AV's view, although their kinematics will continue to be updated. Specifically, we examine three situations with different sectional configurations and varying levels of traffic density, characterized by distinct safety and control mechanisms, and different numbers of initial vehicles. The situations are defined as follows:

- Functional mechanism validation on hard mode: The proposed K-DQN is compared with K-DQN without a safety inspector and without the MPC control module.

Algorithm 3 MPC controller for adjusting EV's velocity

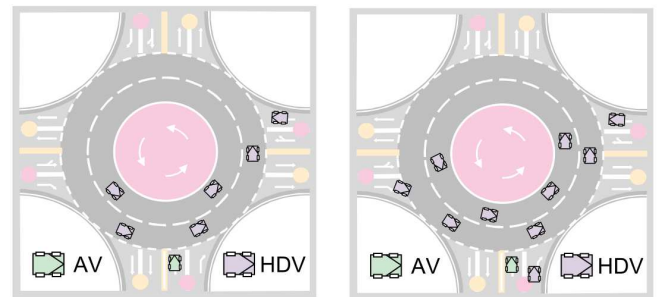
Input: v_{EV}^* : The target speed of the ego vehicle.

Output: $u[0]$: The optimal control input for the first time step, or the output of the PID controller if no solution is found.

```

1: MPC_Controller  $v_{EV}^*$ 
2:  $EV \leftarrow \text{deepcopy}(\text{self})$ 
3:  $N_V \leftarrow \text{get\_surrounding\_vehicles}()$ 
4:  $opti \leftarrow \text{ca.Opti}()$ 
5:  $u \leftarrow opti.variable(N)$ 
6:  $J_c \leftarrow 0$ 
7: for  $k \leftarrow 0$  to  $N - 1$  do
8:   for vehicle in  $NV$  do
9:     action  $\leftarrow \text{use\_K-DQN}$ 
10:     $\_to\_predict\_vehicle\_action(\text{vehicle})$ 
11:   end for
12:    $\delta(k) \leftarrow \text{compute\_steering}(EV, NV)$ 
13:    $EV.update(u(k), \delta(k))$ 
14:    $J_c \leftarrow J_c + (v_{EV}(k) - v_{EV}^*)^2$ 
15:   for  $i \leftarrow 1$  to  $N_v$  do
16:      $J_c \leftarrow J_c + (\|p_{NV}^i(k) - p_{EV}^i(k)\| - D_{safe})^2$ 
17:   end for
18:    $J_c \leftarrow J_c + \lambda u^2(k)$ 
19:    $\text{add\_vehicle\_constraints}(EV, NV, u(k))$ 
20: end for
21:  $opti.minimize(J_c)$ 
22:  $solution \leftarrow opti.solve()$ 
23: if  $solution$  found then
24:   return  $solution.value(u[0])$ 
25: else
26:   return  $\text{PID\_controller}(v_{EV}(0), v_{EV}^*)$ 
27: end if

```



(a) Normal mode settings

(b) Hard mode settings

Fig. 5: Validation settings. (a) is the normal mode settings for the roundabout scenario (six initial HDVs); (b) is the hard mode settings (ten initial HDVs).

- Normal mode validation: The proposed K-DQN is compared with benchmark algorithms with seven initial vehicles in the roundabout as depicted in Fig. 5(a).
- Hard mode validation: The proposed K-DQN is compared with benchmark algorithms with eleven initial vehicles in the roundabout as depicted in Fig. 5(b).

The benchmarks used for comparison in the normal and hard mode validations include PPO [21], A2C [31], ACKTR [32], and DQN [33]. The performance metrics used for evaluation

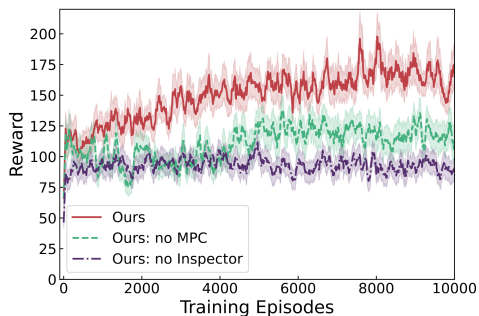


Fig. 6: Curves of reward during training of K-DQN, and K-DQN with no MPC and no inspector, respectively. The shadow region denotes the standard deviations over 3 random seeds. The curve are smoothed over the last 9 evaluation episodes.

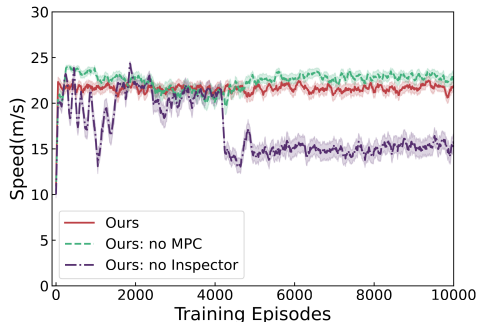


Fig. 7: Curves of speed during training of K-DQN, and K-DQN with no MPC and no inspector, respectively.

include training convergence rate, collision rate, average speed, and reward values during training and evaluation. Considering the inherent risks associated with real-world vehicles and the constraints imposed by legal regulations, scenario-based virtual testing offers significant benefits, such as, precise environmental replication and enhanced testing efficiency. Therefore, this study employs scenarios developed on the Highway virtual simulation platform [34]. At the end of each episode, the vehicles and their velocities are slightly randomized at their spawn points to enhance the generalization capability of our proposed model. The computer and environment setup for this study include Python 3.6, PyTorch 1.10.0, Ubuntu 20.04.6 LTS OS, a 12th generation 16-thread Intel® Core™ i5-12600KF CPU, an NVIDIA GeForce RTX 3090 GPU, and 64GB of RAM.

A. Functional Mechanism Validation

This section describes experiments to evaluate the crucial functions of the safety inspector and MPC of the proposed system in hard mode. We divide the experiments into four validations: Validation 1 evaluates training convergence of K-DQN, K-DQN without safety inspector, and K-DQN without MPC. Validation 2 tests the stability of the speed variations. Validation 3 compares the reward across the evaluation. Validation 4 analyzes the number of collisions.

Validation 1: Training convergence. To better evaluate performance in the case where surrounding HDVs exhibit random driving behavior, we conducted tests using three random

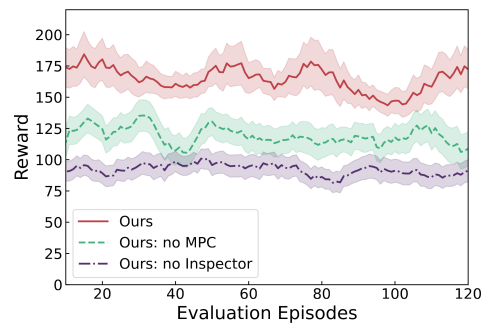


Fig. 8: Curves of reward during evaluation of K-DQN, and K-DQN with no MPC and no inspector, respectively.

TABLE II
COLLISION RATES AND AVERAGE SPEEDS FOR DIFFERENT K-DQN SCHEMES

| Method | No MPC | No Inspector | Ours |
|---------------------|--------------|--------------|----------|
| Collision Rate (%) | 9 | 11 | 1 |
| Average Speed (m/s) | 22.88 | 16.23 | 22.37 |

Collision rate is measured per 100 episodes during training. The best results are highlighted in bold.

seeds and varied the generated scenarios. Fig. 6 illustrates the comparison of training curves between the proposed K-DQN, the K-DQN without a safety inspector, and the K-DQN without MPC. As expected, the proposed K-DQN design outperforms both the K-DQN without a safety inspector and the K-DQN without MPC, delivering higher peak rewards and faster convergence. The training curves of the proposed K-DQN exhibit smooth convergence and low variance across different random seeds, indicating a stable training process. In contrast, the K-DQN without a safety inspector and the K-DQN without MPC show more fluctuations in their training curves and slower convergence rates. It is evident that the absence of a safety inspector leads to the least satisfactory training outcomes. The safety inspector effectively reduces collisions, aligning with the observation that the loss due to collisions is greater than the loss of efficiency during training. The proposed K-DQN surpasses the peak reward of the K-DQN without MPC in approximately 4000 epochs, indicating its superior training performance.

Validation 2: Stability of the speeds variation. Figure 7 illustrates the comparison of speed variation between the proposed K-DQN, the K-DQN without a safety inspector, and the K-DQN without MPC. As expected, the proposed K-DQN design demonstrates more stable speed control compared to the other two networks. It is evident that the absence of a safety inspector leads to the least stable speed variation, resulting in unstable driving. The safety inspector effectively reduces collisions, which aligns with the observation that collisions result in zero-speed events, significantly decreasing the average speed. The K-DQN without MPC exhibits a speed variation around 5 m/s. In contrast, the proposed K-DQN limits the variation to within 2 m/s, enhancing stability.

Validation 3: Reward values among evaluation. Figure 8 illustrates the comparison of rewards between the proposed

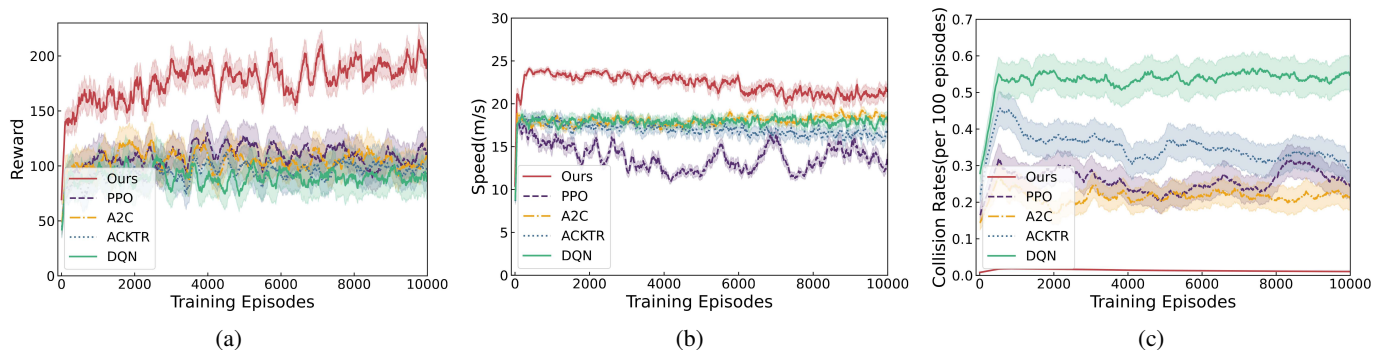


Fig. 9: Comparison of our performances with SOTA algorithms during 10000 training episodes on normal mode scenario. (a) comparison reward ascending during training (b) comparison speed change rate during training, and (c) comparison collision rate change during training.

K-DQN, the K-DQN without a safety inspector, and the K-DQN without MPC. As expected, the proposed K-DQN design demonstrates significantly higher rewards compared to both the K-DQN without a safety inspector and the K-DQN without MPC. The absence of a safety inspector results in the lowest rewards (below 100) because the AV collides with HDVs when it interacts with environment during the training episodes without actions inspector to replace dangerous actions. The K-DQN without MPC increases the reward to around 125 compared to the K-DQN without a safety inspector. However, the proposed K-DQN achieves rewards around 175 in most sections throughout the evaluation episodes.

Validation 4: Collision rate. Table II illustrates the number of collisions and the average speed comparison between the proposed K-DQN, the K-DQN without a safety inspector, and the K-DQN without MPC. As expected, the proposed K-DQN design demonstrates significantly fewer collisions while maintaining a relatively high average speed compared to both the K-DQN without a safety inspector and the K-DQN without MPC. It is evident that the absence of a safety inspector results in the lowest average speed and the highest collision rate. The K-DQN without MPC increases the average speed to 22.88 m/s compared to the K-DQN with a safety inspector, which has an average speed of 16.23 m/s. However, the collision rates for the K-DQN without a safety inspector and the K-DQN without MPC are nearly the same, at 0.11 and 0.09, respectively. The proposed K-DQN achieves a collision rate of 0.01, which is significantly lower than the other two comparison algorithms.

B. Normal Mode Validation

In this section, we conduct experiments to evaluate the safety and efficiency of the proposed system in normal mode compared to other benchmark DRL algorithms, PPO [21], A2C [31], ACKTR [32], and DQN [33]. We divide the experiments into two validations: Validation 1 evaluates fast-convergence training, stable and high-speed variation, and collision rate during training. Validation 2 compares the reward levels during evaluation.

Validation 1: Better training performance. To evaluate the training performance of the proposed K-DQN compared to other benchmark algorithms, we conducted tests using three random seeds and varied the generated scenarios. Fig. 9

illustrates the comparison of training curves between the proposed K-DQN and other benchmark algorithms. Fig. 9(a) shows the comparison of rewards during training, where the proposed K-DQN design outperforms other benchmark algorithms, achieving much higher peak rewards and faster convergence. The DQN has the poorest performance, with rewards around 80. The A2C and ACKTR exhibit similar reward levels, while the PPO reaches approximately 125, the highest reward among the other benchmark algorithms. The proposed K-DQN surpasses all, achieving rewards over 200. Fig. 9(b) depicts the comparison of speed variation during training. The proposed K-DQN design excels, maintaining higher speeds and stable speed variation at the end of training. The PPO demonstrates both the lowest speed and the most unstable speed variation. The A2C, ACKTR, and DQN have similar curves, with the A2C reaching a higher speed of around 18 m/s by the end of 10,000 training episodes. The proposed K-DQN maintains a speed level of approximately 22 m/s at the end, significantly faster than the others. Fig. 9(c) shows the collision rate during training, where the proposed K-DQN design again outperforms the benchmark algorithms by achieving a much lower collision rate. The DQN has the highest collision rate at around 0.55. The ACKTR reduces the collision rate to around 0.35. The A2C and PPO have similar collision rates at around 0.2, with the PPO exhibiting greater variability. The proposed K-DQN maintains a collision rate below 0.05, significantly lower than the others.

Validation 2: Reward values among evaluation. Figure 11 illustrates the reward comparison between the proposed K-DQN and other benchmark algorithms. The proposed K-DQN design demonstrates significantly higher rewards compared to all other benchmark algorithms. The DQN has the lowest reward during the evaluation, falling below 75. The A2C and ACKTR are similar, both increasing the reward to around 75. The PPO has a relatively higher reward of around 100, peaking at 125. However, the reward of the proposed K-DQN fluctuates around 175, significantly surpassing other benchmark algorithms.

C. Hard Mode Validation

In this validation, we rigorously assess the proposed system's driving safety and efficiency within the most challenging

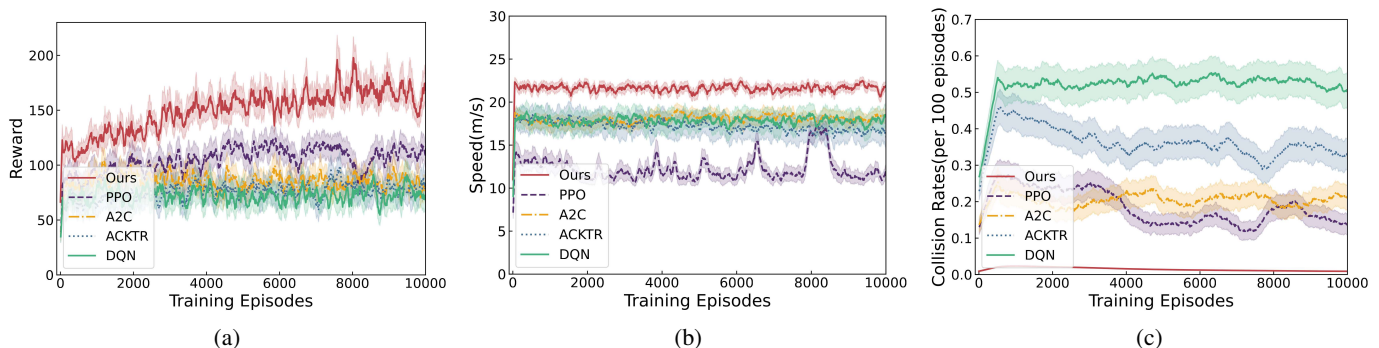


Fig. 10: Comparison of our performances with SOTA algorithms during 10000 training episodes on hard mode scenario. (a) comparison reward ascending during training, (b) comparison speed change rate during training, and (c) comparison collision rate change during training.

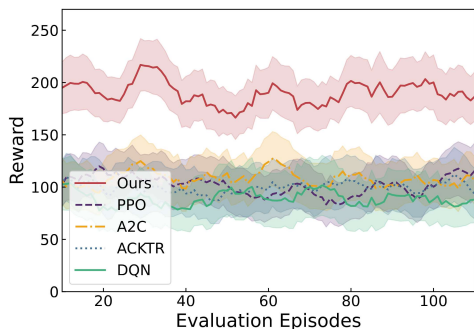


Fig. 11: Curves of reward during evaluation of K-DQN, and benchmark algorithms on normal mode scenario.

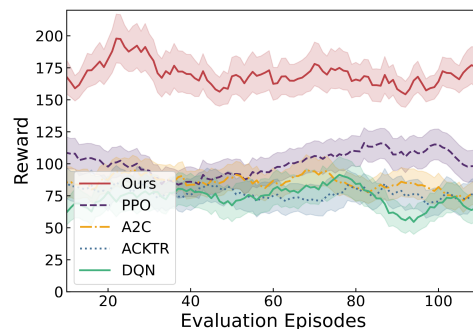


Fig. 12: Curves of reward during evaluation of K-DQN, and benchmark algorithms on hard mode scenario.

operational context. Our methodology contrasts the system’s performance against benchmark algorithms through a two-phase validation process. The first validation focuses on the system’s ability to achieve rapid convergence during training, maintain stability under diverse speed variations, and minimize collision occurrences. The second validation analyzes reward metrics during the evaluation period, highlighting the system’s capacity for optimal decision-making and overall effectiveness during evaluation. Collectively, these validations are designed to substantiate the proposed system’s advanced learning efficiency and robust safety features, positioning it as a superior solution in interactive roundabout driving.

Validation 1: Better training performance. We employed three distinct random seeds to generate a variety of scenarios, ensuring a robust evaluation against other benchmark algorithms. The results, depicted in Fig. 10, reveal a clear superiority of the K-DQN in terms of training performance. Specifically, Fig. 10(a) demonstrates that the K-DQN not only achieved significantly higher peak rewards—approximately 160, compared to the nearest competitor’s 100—but also exhibited a markedly faster convergence rate. In stark contrast, the conventional DQN lagged with rewards near 75. Fig. 10(b) highlights the K-DQN’s proficiency in maintaining both higher and more stable speeds during training, peaking at around 23 m/s, whereas the PPO struggled with the lowest and most erratic speeds, oscillating between 11 m/s and 16 m/s. The A2C, ACKTR, and DQN displayed comparable trajectories,

TABLE III
COLLISION RATES AND AVERAGE SPEEDS FOR THE PROPOSED METHOD AND BENCHMARKS

| Scenarios | Metrics | PPO | A2C | ACKTR | DQN | Ours |
|-------------|----------------|-------|-------|-------|-------|--------------|
| Normal Mode | coll. rate (%) | 23 | 21 | 28 | 52 | 1 |
| | avg. v (m/s) | 14.76 | 18.83 | 17.89 | 18.31 | 21.59 |
| Hard Mode | coll. rate (%) | 12 | 19 | 31 | 52 | 2 |
| | avg. v (m/s) | 13.67 | 18.04 | 17.53 | 17.70 | 22.52 |

coll. rate means collision rate per 100 episodes during training. The best results are highlighted in bold.

with the A2C slightly edging out with speeds up to 18 m/s after 10,000 training episodes. Lastly, Fig. 10(c) underscores the K-DQN’s enhanced safety feature, registering a collision rate below 0.05, a significant reduction compared to the DQN’s 0.52, ACKTR’s 0.35, and the more variable rates of A2C and PPO, which hovered around 0.2 and 0.15, respectively. These findings collectively affirm the K-DQN’s exceptional training efficacy and potential for real-world application due to its high rewards, speed stability, and low collision rates.

Validation 2: Reward values among evaluation. In the conducted evaluation, the proposed K-DQN algorithm’s reward efficacy was benchmarked against conventional algorithms using a triad of random seeds to foster diverse scenario generation, as illustrated in Fig. 12. The empirical data unequivocally demonstrates the K-DQN’s superior reward

acquisition, consistently outperforming its counterparts. The traditional DQN algorithm trailed with suboptimal rewards, not exceeding 70. In contrast, both the A2C and ACKTR algorithms exhibited marginal improvements, hovering around a reward threshold of 75. The PPO algorithm, while achieving a moderate reward peak of 125, generally maintained a reward level around 100. Remarkably, the K-DQN's reward performance remained robust, with a notable fluctuation around 175, thereby establishing its dominance over the other evaluated benchmark algorithms in terms of reward maximization.

Table III provides a comparative analysis of the testing performance for collision rate and average speed between the proposed K-DQN method and four SOTA benchmarks: PPO, A2C, ACKTR, and DQN, evaluated in normal mode and Hard Mode scenarios. In normal mode, the proposed K-DQN demonstrates the lowest collision rate at 0.01, significantly outperforming PPO at 0.23, A2C at 0.21, ACKTR at 0.28, and DQN at 0.52, which indicates the least safe performance by DQN. Additionally, the proposed method records the highest average speed of 21.59 m/s, indicating superior efficiency compared to PPO at 14.76 m/s, A2C at 18.83 m/s, ACKTR at 17.89 m/s, and DQN at 18.31 m/s. In Hard Mode, the proposed K-DQN again shows the lowest collision rate at 0.02, maintaining a clear advantage in safety over PPO at 0.12, A2C at 0.19, ACKTR at 0.31, and DQN at 0.52. It also achieves the highest average speed of 22.52 m/s, demonstrating excellent performance in more challenging scenarios, compared to PPO at 13.67 m/s, A2C at 18.04 m/s, ACKTR at 17.53 m/s, and DQN at 17.70 m/s. The proposed K-DQN consistently shows the lowest collision rate across both modes, underscoring its superior safety mechanisms, and achieves the highest average speed, indicating greater efficiency and stability compared to the benchmark algorithms. The proposed K-DQN consistently shows the lowest collision rate across both modes, underscoring its superior safety mechanisms, and achieves the highest average speed, indicating greater efficiency and stability compared to the benchmark algorithms.

In this study, we have used the average speed of vehicles as a key performance indicator, which serves as an indirect measure of the roundabout capacity. Higher average speeds generally indicate a more efficient flow of traffic and, consequently, a higher capacity. By comparing the average speed of our proposed K-DQN method with benchmark algorithms, we have demonstrated the effectiveness of our approach in improving the overall efficiency and capacity of the roundabout. Among the benchmarks, PPO shows moderate performance but falls behind the proposed method in both collision rate and average speed, while A2C and ACKTR perform better than PPO and DQN but do not reach the performance level of the proposed K-DQN. DQN exhibits the poorest performance in terms of collision rate, though it maintains a relatively high average speed. Overall, the proposed K-DQN method demonstrates significant improvements in both safety, as indicated by lower collision rates, and efficiency, as indicated by higher average speeds, compared to the four benchmark algorithms in both easy and hard driving scenarios, making it highly effective for safe and efficient driving in complex environments.

VII. CONCLUSION

This paper presents a DRL-based algorithm to enhance the safety and efficiency of AVs navigating roundabouts, especially in complex traffic scenarios involving HDVs. By utilizing a DQN capable of processing state information of surrounding vehicles, the system eliminates the need for manual feature engineering and thus enables the AVs to effectively interpret their environment. The integration of a KAN significantly bolsters the AVs' capacity to learn their surroundings with greater accuracy and reliability. The algorithm also incorporates an action inspector to minimize collision risks and a route planner to improve driving efficiency. Additionally, the MPC control ensures the stability and precision of driving actions, contributing to the overall robustness of the system. Evaluations demonstrate the algorithm's superior performance, consistently achieving safe and efficient driving across varying traffic flows. Compared to state-of-the-art benchmark algorithms, the proposed algorithm shows a notable reduction in collision incidents, decreased travel times, and accelerated training convergence rates. Future research will aim to: 1) test our algorithm's robustness in more unpredictable traffic scenarios, including complex urban ramps and intersections, 2) enhance the driving strategy by integrating further goals such as improved passenger comfort, and 3) expand the algorithm's applicability to include collaborative multi-agent operations, which will help in understanding its performance in team-based and competitive urban traffic situations.

REFERENCES

- [1] Y. H. Yap *et al.*, "An international review of roundabout capacity modelling," *Transport Reviews*, vol. 33, no. 5, pp. 593–616, 2013.
- [2] C. Cisneros *et al.*, "Design of mini roundabouts with adaptive traffic lights to improve vehicular travel times and roundabout capacity in metropolitan cities," in *2022 Congreso Internacional de Innovación y Tendencias en Ingeniería (CONIITI)*, 2022, pp. 1–6.
- [3] E. Polders *et al.*, "Identifying crash patterns on roundabouts," *Traffic Injury Prevention*, vol. 16, no. 2, pp. 202–207, 2015.
- [4] K. Xu *et al.*, "A novel two-lane roundabout model with central cross structure," in *Proc. the 6th International Conference on Universal Village*, 2022, pp. 1–9.
- [5] S. Alkheder *et al.*, "Driver behavior at kuwait roundabouts and its performance evaluation," *IATSS Research*, vol. 44, no. 4, pp. 272–284, 2020.
- [6] C. Badue *et al.*, "Self-driving cars: A survey," *Expert Systems with Applications*, vol. 165, p. 113816, 2021.
- [7] J. Pérez *et al.*, "Autonomous driving manoeuvres in urban road traffic environment: A study on roundabouts," vol. 18, 08 2011.
- [8] O. Boualam *et al.*, "Impact of autonomous vehicles on roundabout capacity," *Sustainability*, vol. 14, no. 4, p. 2203, 2022.
- [9] H. A. Ignatious *et al.*, "An overview of sensors in autonomous vehicles," *Procedia Computer Science*, vol. 198, pp. 736–741, 2022.
- [10] A. Deluka Tibljaš, T. Giuffrè, S. Surdonja, and S. Trubia, "Introduction of autonomous vehicles: Roundabouts design and safety performance evaluation," *Sustainability*, vol. 10, no. 4, p. 1060, 2018.
- [11] E. Galceran, A. G. Cunningham, R. M. Eustice, and E. Olson, "Multi-policy decision-making for autonomous driving via changepoint-based behavior prediction," in *Robotics: Science and Systems*, vol. 1, no. 2, 2015, p. 6.
- [12] Q. Ma, X. Wang, S. Zhang, and C. Lu, "Distributed self-organizing control of cavs between multiple adjacent-ramps," *IEEE Trans. Intell. Transp. Syst.*, vol. 24, no. 5, pp. 5430–5441, 2023.
- [13] G. Chen *et al.*, "Secure and safe control of connected and automated vehicles against false data injection attacks," *IEEE Trans. Intell. Transp. Syst.*, vol. DOI: 10.1109/TITS.2024.3371072, 2024.
- [14] P. Hang *et al.*, "An integrated framework of decision making and motion planning for autonomous vehicles considering social behaviors," *IEEE Trans. Veh. Technol.*, vol. 69, no. 12, pp. 14458–14469, 2020.

- [15] S. Pruekprasert *et al.*, “A game-theoretic approach to decision making for multiple vehicles at roundabout,” *arXiv preprint arXiv:1904.06224*, 2019.
- [16] X. Wang *et al.*, “Comprehensive safety evaluation of highly automated vehicles at the roundabout scenario,” *IEEE Trans. Intell. Transp. Syst.*, vol. 23, no. 11, pp. 20 873–20 888, 2022.
- [17] J. F. Medina-Lee *et al.*, “Speed profile generation strategy for efficient merging of automated vehicles on roundabouts with realistic traffic,” *IEEE Trans. Intell. Veh.*, vol. 8, no. 3, pp. 2448–2462, 2023.
- [18] E. Debada *et al.*, “Occlusion-aware motion planning at roundabouts,” *IEEE Trans. Intell. Veh.*, vol. 6, no. 2, pp. 276–287, 2021.
- [19] R. Tian *et al.*, “Game-theoretic modeling of traffic in unsignalized intersection network for autonomous vehicle control verification and validation,” *IEEE Trans. Intell. Transp. Syst.*, vol. 23, no. 3, pp. 2211–2226, 2020.
- [20] K. Yang *et al.*, “Towards robust decision-making for autonomous driving on highway,” *IEEE Trans. Veh. Technol.*, vol. 72, no. 9, pp. 11 251–11 263, 2023.
- [21] B. Peng *et al.*, “Communication scheduling by deep reinforcement learning for remote traffic state estimation with bayesian inference,” *IEEE Trans. Veh. Technol.*, vol. 71, no. 4, pp. 4287–4300, 2022.
- [22] P. Wang *et al.*, “Automated driving maneuvers under interactive environment based on deep reinforcement learning,” *arXiv preprint arXiv:1803.09200*, 2018.
- [23] G. Basile *et al.*, “DDPG based end-to-end driving enhanced with safe anomaly detection functionality for autonomous vehicles,” in *Proc. IEEE MetroXRaine 2022*, 2022, pp. 248–253.
- [24] F. Ye *et al.*, “Automated lane change strategy using proximal policy optimization-based deep reinforcement learning,” in *Proc. the IEEE Intelligent Vehicles Symposium*, 2020, pp. 1746–1752.
- [25] L. Li *et al.*, “Traffic signal timing via deep reinforcement learning,” *IEEE/CAA Journal of Automatica Sinica*, vol. 3, no. 3, pp. 247–254, 2016.
- [26] G. Dulac-Arnold *et al.*, “Deep reinforcement learning in large discrete action spaces. arxiv 2015,” *arXiv preprint arXiv:1512.07679*.
- [27] Z. Liu, Y. Wang, S. Vaidya, F. Ruehle, J. Halverson, M. Soljačić, T. Y. Hou, and M. Tegmark, “Kan: Kolmogorov-arnold networks,” *arXiv preprint arXiv:2404.19756*, 2024.
- [28] M. M. Minderhoud and P. H. Bovy, “Extended time-to-collision measures for road traffic safety assessment,” *Accident Analysis & Prevention*, vol. 33, no. 1, pp. 89–97, 2001.
- [29] L. Schumaker, *Spline Functions: Basic Theory*, 3rd ed. Cambridge: Cambridge University Press, 2007.
- [30] S. Beamer *et al.*, “Direction-optimizing breadth-first search,” in *Proc. the International Conference on High Performance Computing, Networking, Storage and Analysis*. IEEE, 2012, pp. 1–10.
- [31] B. Peng *et al.*, “Adversarial advantage actor-critic model for task-completion dialogue policy learning,” in *IEEE International Conference on Acoustics, Speech and Signal Processing*. IEEE, 2018, pp. 6149–6153.
- [32] Y. Chu, Z. Wei, G. Sun, H. Zang, S. Chen, and Y. Zhou, “Optimal home energy management strategy: A reinforcement learning method with actor-critic using kronecker-factored trust region,” *Electric Power Systems Research*, vol. 212, p. 108617, 2022.
- [33] P. Cai *et al.*, “Dq-gat: Towards safe and efficient autonomous driving with deep q-learning and graph attention networks,” *IEEE Trans. Intell. Transp. Syst.*, vol. 23, no. 11, pp. 21 102–21 112, 2022.
- [34] E. Leurent, “An environment for autonomous driving decision-making,” <https://github.com/eleurent/highway-env>, 2018.